IEEE Access
Multidisciplinary ⋮ Rapid Review ⋮ Open Access Journal

Received 27 November 2023, accepted 23 December 2023, date of publication 25 December 2023,
date of current version 5 January 2024.

Digital Object Identifier 10.1109/ACCESS.2023.3347425

RESEARCH ARTICLE

Detection of Series Arcs in Low-Voltage AC Power Lines Using Load Side Voltage Sag and Waveform Similarity Comparison

KAIJIE WANG[1], XIANGNING LIN[1], (Senior Member, IEEE), FANRONG WEI[1], AND HU WEI[2]

[1]State Key Laboratory of Advanced Electromagnetic Engineering and Technology, School of Electrical and Electronic Engineering, Huazhong University of Science and Technology, Wuhan 430074, China
[2]State Grid Hubei Electric Power Research Institute, State Grid Hubei Electric Power Company Ltd., Wuhan 430077, China

Corresponding author: Fanrong Wei (610300307@qq.com)

This work was supported by the National Key Research and Development Program of China under Grant 2022YFE0120400.

ABSTRACT The similarity between arc fault current waveforms and nonlinear load currents can lead to misjudgments in arc fault identification methods that rely on arc current. In response to this issue, this paper establishes a unified fault criterion based on the conclusion that different types of loads that exhibit similar magnitudes of load side voltage sag during arc faults. Combined the voltage sag criterion with waveform criteria, this paper proposes a novel arc fault detection method. The method takes the load side voltage sag value exceeding the threshold as the detection start condition. After detection starts, the method identifies faults by calculating the degree of load side voltage waveform distortion using Hausdorff distance algorithm. Simulations are conducted on five different loads to determine the startup threshold and detection threshold. Test results show that the fault identification accuracy of the proposed method is 100% under the above thresholds.

INDEX TERMS Series arc fault, arc voltage, voltage sag, Hausdorff distance.

I. INTRODUCTION

The ignition of distribution circuits is a significant cause of electrical fires, with over 40% of electrical fires annually originating from electrical circuitry. Among these incidents, series arc faults caused by loose terminals, insulation damage, and conductor impairment stand out as one of the primary triggers for distribution line fires [1]. In response to this hidden danger, the National Electrical Code (NEC) in the USA introduced a mandate through the UL1699 standard for the implementation of arc fault circuit interrupters (AFCI) in electrical installations operating on 110 V/60 Hz power grids in 2002, aiming to bolster their protection. With the 2022 updates to the UL1699 standard, it is now compulsory to incorporate AFCIs in all residential electrical installations [2]. Chinese national standard GB 14287.4-2014 specifies the terms and definitions, classification, requirements, tests, inspection rules, markings, and instructions for arcing fault detectors installed in electrical circuits of 10 kW and below in industrial and civil buildings [3].

The arc faults are a major issue not only in high-voltage power grids [4], but also in smart DC (mainly photovoltaic) [5] and low-voltage distribution systems [6]. Methods for detecting AC series arc faults in low-voltage distribution systems can be categorized as follows: (1) Detection methods based on physical characteristics of arc such as sound, light, and magnetism. This method requires the installation of sensors near the potential locations of arc faults so its detection range is limited. It is commonly used in switchgear and difficult to identify arc faults in dispersed electrical equipment and wiring [7]. (2) Detection methods based on electrical characteristics. These methods achieve fault detection by extracting features from fault current waveforms. It can be used to detect faults occurring on dispersed electrical equipment and wiring, making it become research focus in series arc fault detection for power lines [8].

When a protected line experiences an arc fault, the arc extinguishes near the zero crossing of the current, and

The associate editor coordinating the review of this manuscript and approving it for publication was Arturo Conde.

a ''zero rest'' phenomenon occurs in the current. During the zero rest period, high-frequency components appear, which can be used as a criterion for determining whether an arc fault has occurred [9], [10]. However, under the condition of nonlinear load, it can also appear ''zero rest'' when the arc fault does not occur, which easily causes misjudgment. The research work presented in [11], [12], [13], and [14] utilize signal processing methods to detect the singularity of fault currents, which has high detection sensitivity. However, the harmonic content of distribution network current is high, and the current waveform itself has certain singularity, which is also prone to misjudgment. With the advancement of intelligent detection technology, alternative approaches to identify fault current characteristics involve the application of artificial intelligence algorithms. The research work presented in [15], [16], [17], and [18] employ artificial intelligence techniques to conduct reinforcement learning on precollected arc current data, followed by using the well-trained model for arc fault detection. These methods place high demands on the computational performance of IED (Intelligent Electronic Devices). Moreover, confirmation is still needed regarding the method's generalization capabilities for diverse kinds of loads. Currently, its engineering practical value needs further evaluation.

The major drawback of arc fault detection methods based on arc current characteristics lies in the substantial existence of nonlinear loads, causing normal load currents during regular operation to present similar fault characteristics as arc currents, leading to misjudgment, which makes it difficult to meet the demands for accurate arc fault identification. As a result, researchers and professionals have in recent years begun to explore detection methods using arc voltage characteristics. The research work presented in [19] addresses the challenge of identifying mixed loads by employing wavelet packet transform to process arc fault voltages, partially solving the problem resulting from mixed loads. However, the choice of different wavelet bases significantly has strong impacts on the detection results. The research work presented in [20] uses harmonics generated by arc voltage to detect arc fault. However, the experimental loads are not enough to verify the effectiveness of the method. The research work presented in [21] introduces a differential voltage detection method using upstream and downstream dual monitoring points. It detects faults by analyzing the voltage changes between these points, offering a promising solution. However, it requires synchronously sampling in multiple points, which limits its applicability in low-voltage distribution networks. Artificial intelligence technique also has been introduced to detect arc fault voltage [22]. But it has the same drawback as mentioned in [15], [16], [17], and [18].

In response to the challenges existing in series arc fault detection as described above, an in-depth analysis of the influence of arc resistance on the load-side voltage is conducted by establishing a mathematical description of series arc faults. Furthermore, a novel method for arc fault detection is proposed based on voltage sag characteristics and the Hausdorff waveform similarity algorithm.In this method, the voltage sag value on the load side is used as a triggering condition. The detection process involves calculating the Hausdorff similarity between the arc voltage waveform and a sine waveform to determine the occurrence of a series arc fault. Finally, an arc simulation model is established using MATLAB/Simulink to validate the effectiveness of the proposed detection method through simulations. This method is expected to address the difficulties posed by existing methods in recognizing nonlinear loads.

II. ARC FAULT DETECTION BASED ON LOAD SIDE VOLTAGE SAG

A. ANALYSIS OF FAULT CHARACTERISTICS OF SERIES ARC

Arc is a high-temperature, high-brightness discharge phenomenon usually caused by gas discharge between two electrodes. Arcs can be divided into three stages: arc ignition, arc combustion, and arc extinction. Gas discharges occur when a sufficient voltage is applied between the electrodes, ionizing the gas around the electrode surfaces and forming a plasma cloud. This process is known as ''arc ignition''. During this stage, the arc current is low, and the resistance between the electrodes is high.

In the arc burning stage, both the arc current and temperature rapidly increase. Since a millimeter-scale gap is enough to extinguish the arc, the distance between the two contacts in a series arc must be very close to maintain combustion. This allows us to ignore the arc column voltage drop and consider the arc voltage drop as dependent on the near-electrode region voltage drop. And when the arc is stably burning, its voltage drop does not vary much with current, allowing it to be approximated as a constant. For air as the medium, commonly used copper electrode materials can be assumed as $U_0 \approx 20V$ [23]. As the current decreases, the arc enters the arc extinction stage, continuing until the arc is completely extinguished, accompanied by the sharp increase of the resistance between the electrodes.

Based on the analysis above, in the case of a series arc fault occurring in low-voltage distribution lines, it can be regarded as a non-linear resistor connected in series in the line. The resistance value of this resistor varies with the current and changes during the arc burning, with a variation period of half a cycle. According to the arc discharge process, the arc resistance can be divided into 3 stages. $0-t_1$ represent the arc ignition stage. t_1-t_2 and t_3-t_4 represent the arc combustion stage. t_2-t_3 represents the arc extinction and re-ignition stage. t_4-0.02s represents the arc extinction stage. In the arc combustion stage, the rate of change of arc resistance is relatively small and tends to stabilize. In the arc extinction and ignition stage, the rate of change of arc voltage is significant, while the arc current is nearly zero, causing the arc resistance to approach infinity.

During the arc combustion stage, the arc resistance undergoes relatively small variations and can be approximated as a constant, affected by the load. Using the minimum arc

resistance represents the resistance value of this stage. Based on the simulation results, arc resistance in combustion stage can be represented as a function of the load through fitting function as follows.

$$\begin{cases} R_{\min} = R_{arc}(t) = 0.113R + 0.00072X^2 \\ (t_1 < t \le t_2, t_3 < t \le t_4) \end{cases} \quad (1)$$

where R represents load resistance and X represents load reactance.

The resistance of the arc during the arc ignition and extinction stages can be obtained from the Cassie arc model [24]:

$$\frac{d \ln g}{dt} = \frac{1}{\tau}\left(\frac{u^2 - U_c^2}{U_c^2}\right) \quad (2)$$

where arc resistance $R_{arc}(t) = {}^1/_g$,τ represents the arc time constant, u represents arc voltage, and U_c represents the arc voltage constant. For the sake of convenience, the arc extinction and reignition stage between t_2 and t_3 was selected for arc resistance calculation. After integrating both sides, we can obtain the formulas for the arc resistance during the arc ignition and extinction stages.

$$R_{arc}(t) = \frac{1}{e^{\frac{1}{\tau}(\int_{t_2}^{t} dt + \frac{1}{U_c^2}\int_{t_2}^{t} u^2 dt)}} \quad (3)$$

When the current is in the "zero rest" phase, the recovery voltage across the arc gap can be neglected. Assuming a moment in time, denoted as $t = t_2$, when an arc fault occurs in the circuit, and considering that the arc resistance cannot undergo a sudden change, $R_{arc}(t) = R(t_2)$ is met at this time, the equation for $R_{arc}(t)$ during the extinction stage is as follows:

$$R_{arc}(t) = R_{\min}\frac{1}{e^{\frac{1}{\tau}(t_2 - t)}}, t_2 \le t < 0.01s \quad (4)$$

where $R_{\min}$ represents the initial resistance value during extinction.

Similarly, the resistance during the arc reignition can be expressed as:

$$R_{arc}(t) = R_{\max}\frac{1}{e^{\frac{1}{\tau}(t_3 - t)}}, 0.01s \le t < t_3 \quad (5)$$

where $R_{\max}$ represents the maximum value during arcs. $R_{\max}$ can be approximated by the following fitting function.

$$R_{\max} = R_{arc}(t = 0.01s) = 3620R + \frac{8100}{X}R^2 - 2440X \quad (6)$$

The resistance of the arc in the arc ignition, combustion, and extinction stages can be segmented as follows:

$$R_{arc}(t) = \begin{cases} 0.113R + 0.00072X^2, 0 < t < t_1 \\ R_{\min}\frac{1}{e^{\frac{1}{\tau}(t_2 - t)}}, t_2 < t < 0.01s \\ R_{\max}\frac{1}{e^{\frac{1}{\tau}(t_4 - t)}}, 0.01s < t < t_3 \end{cases} \quad (7)$$

It is noted that the arc resistance in the extinguishing-arc stage in Equation (7) changes exponentially. And the arc time constant is usually very small, on the order of 10^-4s [24],

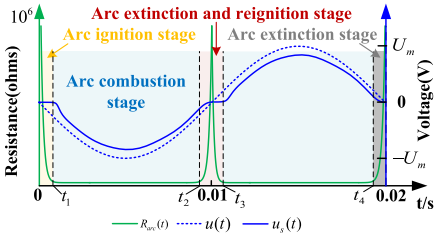

FIGURE 1. Schematic diagram of arc voltage and arc resistance.

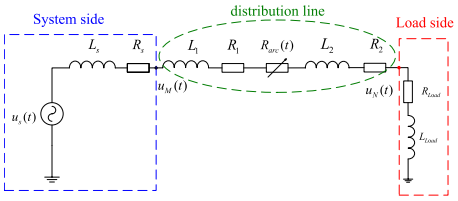

FIGURE 2. Series arc fault equivalent circuit.

which means that the arc resistance in this stage will rise to over 10^4 ohms in a very short time. Therefore, the arc current is almost zero for most of the time in this stage. To facilitate the analysis of load side voltage influenced by arc resistance, the expression of arc resistance in Equation (7) is simplified to obtain the segmented expression of arc resistance represented by half-cycle as shown in Equation (8).

$$R_{arc}(t) = \begin{cases} \infty, 0 < t \le t_1 \\ 0.113R + 0.00072X^2, t_1 < t \le t_2 \\ \infty, t_2 < t \le 0.01s \end{cases} \quad (8)$$

The access of arc resistance $R_{arc}(t)$ will have an impact on the magnitude of the load terminal voltage. Uses $u_s(t) = -U_m \sin(100\pi t)$ represent the system side voltage, $u(t)$ represent load side voltage. Figure 1 depicts the schematic diagram of the phase relationship between voltage $u(t)$, $u_s(t)$ and arc resistance $R_{arc}(t)$. Assuming no energy storage components existing on the load side, and neglecting the line voltage drop.

As shown in figure 1, during the arc ignition $(0 - t_1)$ and arc extinction stages $(t_2 - 0.01)$ depicted in the diagram, the arc resistance is effectively infinite, rendering the circuit effectively open, and since there are no energy storage components at the load side, the voltage on the load side is 0.

However, during the arc combustion stage $(t_1 - t_2)$, as the equivalent resistance of the arc $R_{arc}(t)$ is relatively small, the voltage drop across the arc resistance is relatively small too. As a result, the load side voltage exhibits a sine waveform with an amplitude lower than that of the system side voltage.

B. ARC FAULT DETECTION BASED ON LOAD SIDE VOLTAGE SAG

The influence of series arc resistance on voltage distribution can be reflected in the phase voltage of the faulted phase, therefore, theoretical analysis can be conducted using a single-phase system. The equivalent circuit for a series arc fault is depicted in Figure 2.

Among which, the point of connection between the distribution network and the power grid can be considered to have a grid voltage unaffected by the load. In the analysis of arc faults, the voltage at this point can be equivalently represented as a constant voltage source $u_s(t)$ of 220V. The magnitude of the system side voltage $u_M(t)$ is equal to the value of the grid voltage substracted by the voltage drop across the impedance of the system side line, as given by:

$$u_M(t) = u_s(t) - i(t)R_s - L_s\frac{di(t)}{dt} \tag{9}$$

During an arc fault, an equivalent nonlinear resistor $R_{arc}(t)$ is introduced into the circuit, resulting in a reduction in the RMS value of the current *i(t)*. For the system side voltage $u_M(t)$, due to the fact that the impedance of the system side line is typically less than 5% of the total circuit impedance, the voltage drop on the system side caused by current reduction generally does not exceed 1V. Consequently, the fault voltage sag is not very pronounced. As a result, the fault cannot be detected effectively on relying on the system side voltage $u_M(t)$.

However, for the load-side voltage $u_N(t)$, before the fault occurrence, it is determined as the system side voltage $u_M(t)$ minus the voltage drop across the line impedance, as given by equation (10). After an arc fault, an equivalent nonlinear resistor is introduced into the circuit, and the load-side voltage $\acute{u}_N(t)$ is calculated as the system side voltage $u_M(t)$ minus the combined voltage drops across the line impedance and the arc resistance, as shown in Equation (11).

$$u_N(t) = u_s(t) - i(t)(R_s + R_1 + R_2) - (L_s + L_1 + L_2)\frac{di(t)}{dt} \tag{10}$$

$$u'_N(t) = u_s(t) - i(t)(R_s + R_1 + R_2 + R_{arc}(t)) - (L_s + L_1 + L_2)\frac{di(t)}{dt} \tag{11}$$

Due to the fact that the resistance of the arc is greater than the line resistance, a noticeable voltage division occurs during the arc fault. During an arc fault, there is an evident arc fault voltage drop of about 15-20V at the location of the arc occurrence. The voltage drop across the line equals the sum of the normal line voltage drop and the arc voltage. As a result, at the load-side monitoring point, a voltage sag of around 15-25V occurs. The fault voltage detected at the load side falls below the voltage range during normal operation. This voltage sag due to the arc fault is very distinct.

From the above analysis, it becomes evident that a discrepancy exists in voltage magnitudes between the system side voltage and the load side voltage when a series arc fault occurs in a low-voltage distribution line. Consequently, if the difference between the load side voltage magnitude during such a fault and the load side voltage magnitude during normal operation can be detected, it becomes possible to address the challenge of distinguishing between the operation of nonlinear loads and series arc faults.

III. ANALYSIS OF VOLTAGE SAG CHARACTERISTICS AT THE LOAD-SIDE

Although voltage sag at the load side is a significant feature of series arc faults, it is important to note that there are various causes of voltage sags in low-voltage distribution networks. Therefore, for the purpose of exploring the feasibility of utilizing this phenomenon for the purpose of detecting arc faults, it is necessary to conduct in-depth research into the characteristics of load side voltage sags in low-voltage distribution networks.

In actual systems, the main factors contributing to significant voltage sags include system short-circuit faults (FRS, Fault Related Sags), as well as scenarios like heavy load startup and induction motor starting [25], [26]. Among these, FRS events are characterized by their long propagation distance, large sag amplitude, and rapid drop and recovery. Considering that short-time delay overcurrent release in distribution networks usually respond promptly to system short-circuit faults, it can be assumed that the short-time delay over-current release in the distribution network takes action before the arc fault detection devices. Therefore, the influence of voltage sag phenomena due to system short-circuit faults on arc fault identification is not considered in this paper.

Scenarios causing voltage sags during normal operation of the system include instances like heavy load access and asynchronous motor starting. Compared to short-circuit faults, the voltage sag amplitudes resulting from these factors are generally smaller, but they can persist for longer durations.

To determine whether voltage sags resulting from actions like heavy load switching and asynchronous motor starting could lead to misjudgment of arc fault detection methods based on voltage sags, it is necessary to conduct a comparative analysis among the voltage sag phenomena during heavy load accessing, asynchronous motor starting, and the voltage sag phenomena during the occurrence of arc faults.

TABLE 1. Low-voltage distribution network cable parameters.

Cable model	Bore size(mm^2)	Resistance(/km)	inductance (mH/km)	Rated current(A)
KVV/KVVP	4	5	1	10
RVV/RVVP	6	2.66	0.98	15
BV/BVR	10	1.6	0.95	25
RV/RVB	16	1	0.8	35

In low-voltage distribution networks, the supply radius is generally short, and the line impedance is low. Considering the low-voltage distribution network cable parameters presented in Table 1 and using Equation (10) to calculate the voltage drop based on the cable's rated current, it is found that:

According to the requirements of low-voltage distribution network design standards, when the distribution network line reaches a maximum distance of 250m, the line voltage drop does not exceed 6V. Build the circuit shown in Figure 2 in MATLAB/Simulink, use impedance Z_s connected to constant

voltage source to simulate the voltage drop on the system side. The distribution branch uses $4mm^2$/100m cable in Table 1, and the distribution trunk uses $10mm^2$/150m cable in Table 1. Based on the above setup, simulate line overload by changing the load power. The simulation results show that the load access voltage drop in this extreme scenario is 8.166V. This value is still smaller than the voltage sag caused by series arc faults. Therefore, it is possible to distinguish between heavy load switching and arc faults by setting appropriate threshold values.

It should be pointed out that, nonlinear loads such as power electronic loads are prone to misjudgment in arc detection methods based on current waveforms due to the high harmonic content of their working current. However, in the proposed method, the voltage sag during the access of such loads will not exceed the starting threshold, and the detection will not start. This is because no matter how variable the current waveform of a nonlinear load is, the RMS of its current only depends on its power, resulting in a relatively constant voltage sag. Simply put, the voltage sag values of a 1000W linear load and a 1000W nonlinear load should be similar, and nonlinear loads will not bring additional difficulties to detection. In summary, the proposed method has found a way to avoid misjudgment caused by nonlinear loads.

If a large-capacity asynchronous motor is accessed to the load side and is started at full voltage, the starting current can reach a value of 500% to 800% of the full load current. During the initial moments of starting, the current can exceed the rated current of the cable. When this high current passes through the line impedance, it causes a drop in voltage, resulting in a voltage sag phenomenon. This type of voltage sag is known as MSRS (Motor Starting Related Sags), which are related to the starting of electric motors [27], [28]. In direct starting of asynchronous motor, the voltage sag is most severe during the initial moment of starting. The load-side voltage experiences a substantial voltage sag, which then gradually rises as the motor speed increases.

Considering a calculation based on an extreme starting current of 8 times the rated current, for example, in the case of a 4kW motor with a rated speed of 1430 RPM, the voltage sag amplitude during motor starting can reach up to 15V. This amplitude is similar to the voltage sag amplitude during an arc fault. In this scenario, the methods relying on voltage sag values only to differentiate between asynchronous motor starting and arc faults could lead to misjudgments.

From the analysis above, it can be concluded that setting a sag threshold can help differentiate between the voltage sags caused by common non-asynchronous motor loads and those caused by arc faults. However, relying solely on voltage sag characteristics is not effective in distinguishing between asynchronous motor starting and arc faults. Therefore, it is necessary to further integrate information regarding the amplitude of load-side voltage sags and the waveform characteristics of load-side voltage to accurately identify arc faults.

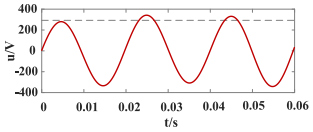

(a) Voltage waveform of asynchronous motor starting

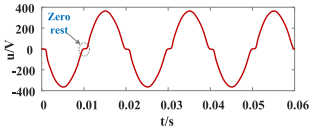

(b) Phase voltage waveform of arc fault

FIGURE 3. The load-side voltage waveform of asynchronous motor starting and series arc fault.

IV. A METHOD FOR SERIES ARC FAULT DETECTION BASED ON VOLTAGE SAG CHARACTERISTICS AND HAUSDORFF SIMILARITY

To address the problem where voltage sag values during asynchronous motor starting closely resemble those during arc faults, it is necessary to utilize the fault waveform characteristics to further distinguish between above scenarios, and an arc fault detection algorithm that combines voltage sag features with waveform characteristics is proposed correspondingly.

A. IDENTIFICATION OF ASYNCHRONOUS MOTOR STARTING AND SERIES ARC FAULTS BASED ON HAUSDORFF DISTANCE ALGORITHM

During an arc fault, the load-side voltage will significantly deviate from a sinusoidal waveform, as shown in Figure 1. This deviation is primarily characterized by the appearance of a step or discontinuity at a certain position in the voltage waveform. The specific waveform changes vary based on different load types.

During the starting of an asynchronous motor, the load-side voltage is equal to the value of the grid voltage minus the voltage drop across the line impedance, as given by equation (10). While the distorted current waveform can introduce a slight distortion in the load-side voltage waveform due to the voltage drop across the line resistance, the impedance of low-voltage distribution lines is relatively small. This means that the distortion caused by the voltage drop across the line impedance is limited. As a result, the load-side voltage waveform during asynchronous motor starting approximates a standard sinusoidal waveform, as shown in Figure 3.

Therefore, it is possible to differentiate between asynchronous motor starting and arc faults by analyzing the distorted characteristics of the load-side waveform during arc faults. To detect the degree of distortion in the load-side voltage waveform, this paper proposes a method for fault identification based on the Hausdorff distance algorithm.

Hausdorff distance is a measure of the similarity between two sets of points [29]. Assuming there are two sets of point sets A and B:

$$A = \{a_1, \ldots, a_n\} \tag{12}$$

$$B = \{b_1, \ldots, b_n\} \tag{13}$$

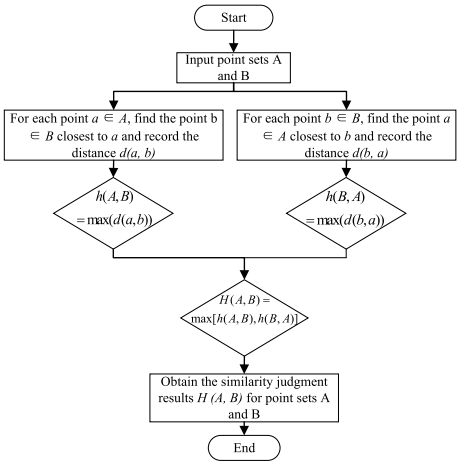

FIGURE 4. Hausdorff distance algorithm calculation flow chart.

Calculate and compare the Euclidean distance between a point in set A (such as a_i) and all points in set B, and find the closest point b_j to a_i, so that b_j satisfies:

$$\left\|a_i - b_j\right\| \leq \|a_i - b_k\|, 1 \leq k \leq n, k \neq j \tag{14}$$

Among them, represents the Euclidean distance between two points. The minimum Euclidean distance of the corresponding point in the above equation is:

$$\min_{b \in B} \|a_i - b\| = \left\|a_i - b_j\right\| \tag{15}$$

For all elements in set A, the maximum value that satisfies equation (16) is the Hausdorff one-way distance from set A to set B, which is:

$$h(A, B) = \max_{a \in A} \min_{b \in B} \|a - b\| \tag{16}$$

By analogy, the Hausdorff one-way distance from set B to set A is:

$$h(B, A) = \max_{a \in B} \min_{b \in A} \|a - b\| \tag{17}$$

Define the Hausdorff distance H (A, B) between point set A and point set B as

$$H(A, B) = \max[h(A, B), h(B, A)] \tag{18}$$

The Hausdorff distance between point sets A and point sets B is the larger of the one-way Hausdorff distances from A to B and from B to A. The Hausdorff distance value H(A,B) is the result of determining the similarity between the two point sets. A larger H(A,B) indicates a lower degree of similarity between point sets A and B. Figure 4 illustrates the calculation process of the Hausdorff distance.

Utilizing the Hausdorff distance algorithm for fault identification involves comparing a template waveform with a measured waveform. Considering the characteristics where arc fault waveforms deviate from sinusoidal and asynchronous motor starting waveforms approximate sinusoidal, this paper chooses a sinusoidal waveform as the template for calculating the Hausdorff distance.

In this method, the criterion is designed by calculating the Hausdorff distance between the load-side voltage waveform and the sinusoidal waveform template. When the load-side voltage waveform undergoes distortion, leading to the Hausdorff distance between the load-side voltage waveform and the standard sinusoidal waveform template exceeding the threshold, an arc fault occurrence is identified successfully.

B. SERIES ARC FAULT DETECTION PROCESS BASED ON VOLTAGE SAG AND HAUSDORFF DISTANCE ALGORITHM

The criterion using voltage sag characteristics for fault identification is simple, with strong universality. Setting it as the triggering condition for detection ensures that detection does not initiate during normal operation, which reduces the frequency of detection start-ups and enhances the accuracy of identification.

To address potential false start-ups caused by excessive voltage sag values during asynchronous motor starting, the Hausdorff distance algorithm calculates the Hausdorff distance between the voltage waveform and the sinusoidal waveform as soon as the detection is initiated. The calculated Hausdorff distance is denoted as ''H value''. It is classified as normal system operation if the load-side voltage sag value exceeds the threshold while the H value remains within the threshold. If both the load-side voltage sag value and the H value exceed their respective thresholds, an arc fault occurrence can be determined.

The concrete detecting process is as follows:

1) Real-time sampling of the load side voltage is conducted based on a sampling frequency of 10kHz, resulting in a sampled array of load side voltage values $u = [u_1, u_2, \cdots, u_n]$. Wherein, the sampling array contains 2 cycles at 50Hz (0.04s), which consist of 400 sampling points ($n = 400$). Additionally, the maximum voltage value $u_{mag} = \max[u_1, u_2, \cdots, u_n]$ within the voltage array is recorded.

2) The root mean square (RMS) value of the load side voltage is calculated, along with the voltage sag value from the present moment compared to the previous power frequency cycle (20ms ago). The calculation formula for load-side voltage sag is as follows:

$$U_{sag}(T) = U(T) - U(T-1) T = 1, 2, 3, \cdots n \tag{19}$$

where, $U_{sag}(T)$ represents the voltage sag value, $U(T)$ is the RMS value of the load-side voltage for the current cycle, and $U(T-1)$ is the RMS value of the load-side voltage for the previous cycle.

Using voltage sag value $U_{sag}(T)$ exceeding a threshold U_{set} as the triggering condition for detection. When an arc fault occurs, the voltage drop should meet the following condition:

$$U_{sag}(T) \geq U_{set} \tag{20}$$

3) Construct a sinusoidal waveform template with an amplitude equal to the load-side voltage amplitude U_{mag}. The mathematical expression for the sinusoidal waveform is $y = U_{mag} \sin(2 * \pi * 50 * t_i)$. Save the sinusoidal values at

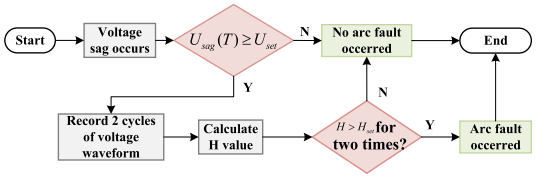

FIGURE 5. Fault detection flow chart.

each time point t_i in an array to obtain a discrete sequence of the standard sinusoidal waveform $y = [y_1, y_2, \cdots, y_n]$.

4) To calculate the H value within a single cycle, it is necessary to align the data moments of the load-side voltage sequence and the standard sinusoidal waveform sequence. Given that both are sinusoidal waveform variations, alignment can be achieved by synchronizing their maximum values. The steps for this process are as follows:

a) Identify the maximum values of both sequences $y = [y_1, y_2, \cdots, y_n]$ and, and record the moment when the maximum value occurs.

b) Calculate the time difference between the moments of the two maximum values, which corresponds to the number of sampling intervals between them.

c) For the waveform with the maximum value occurring earlier, align it with the waveform that has the maximum value occurring later by shifting the data points to the right. The distance of the shift equals the number of sampling points corresponding to the time offset. This process results in the phase-aligned sequences $y' = [y_1, y_2, \cdots, y_n]$ and $u' = [u_1, u_2, \cdots, u_n]$.

5) Calculate the Hausdorff distance between the load-side voltage sequence $u' = [u_1, u_2, \cdots, u_n]$ and the standard sinusoidal waveform sequence $y' = [y_1, y_2, \cdots, y_n]$. Using H_{set} to represent the threshold, the following conditions should be met when an arc fault occurs:

$$H(u', y') > H_{set} \tag{21}$$

where $H(u', y')$ represents the Hausdorff distance between the load-side voltage and the standard sinusoidal waveform, and H_{set} represents the detection threshold.

6) The the detection action delay Δt can be set according to the criterion below: To prevent false detection caused by network short-circuit faults, the action delay Δt should be greater than the operating time of the protection device.

7) If the H-value exceeds the threshold twice within half a cycle of the waveform, which means it is detected twice during a single frequency cycle, the action delay procedure is initiated. When the delay period is reached, a signal indicating fault occurrence is generated.

Figure 5 depicts the detection process flowchart for series arc fault detection based on voltage sag characteristics and the Hausdorff distance algorithm.

C. CRITERIA SETTING

Regarding the setting of the startup threshold U_{set} and the detection threshold H_{set}, the specific value for U_{set} is provided here along with the setting approach for H_{set}. The value setting for H_{set} will be presented in the subsequent simulation experiments.

1) U_{SET} SETTING

Based on the analysis from the previous section, the conclusion can be drawn that the chosen startup threshold U_{set} should effectively identify the voltage sags caused by load connection other than three-phase asynchronous motor starting from the voltage sags due to arc faults. The design of the startup threshold should prioritize reliable detection initiation when an arc fault occurs, even if it results in some permissible false starts due to load connection. Therefore, the reliability coefficient should not be set excessively high, ensuring reliable initiation of protection in the event of an arc fault:

$$U_{set} = U_{\max} \cdot K_{rel} \tag{22}$$

where U_{set} is the startup threshold, $U_{\max}$ is the maximum voltage sag due to load connection, and K_{rel} is the reliability coefficient. The principle of selecting a reliability coefficient is to ensure reliable detection startup reliably when a fault occurs. Moreover, the detection false start caused by normal operating voltage drop can be distinguished from arc faults through Hausdorff distance comparison, so selecting a small K_{rel} will not affect the detection accuracy. Therefore, we select a reliability coefficient of 1.2 here to balance high detection accuracy and few false startup times.

Based on the calculated results, the maximum voltage sag due to load access is 9V. Using equation (22), we can determine that the set startup threshold U_{set} is 10.8V.

2) H_{SET} SETTING

The setting of the detection threshold H_{set} should ensure that it can prevent false triggers under the most adverse conditions of direct starting of asynchronous motors while accurately identifying arc faults.The starting methods of asynchronous motors can be divided into direct starting and partial voltage start. Usually, for residential buildings analyzed in this paper, there will not be high-power asynchronous motors on the load side. For small asynchronous motors, the starting method used is direct starting. Therefore, the authors take the maximum asynchronous motor capacity (7.5kW) that allows direct starting as the research object to determine Hmax. We use the H value of the starting of the 7.5 kW asynchronous motor as $H_{\max}$, and then multiply it by the reliability coefficient K_{rel2} to set the detection threshold H_{set}.

$$H_{set} = H_{\max} \cdot K_{rel2} \tag{23}$$

where $H_{\max}$ is the maximum H value during the starting process of the asynchronous motor; K_{rel2} is the reliability coefficient.

Based on the waveform analysis in Section III, it can be found that the degree of waveform distortion during arc faults is much greater than that during asynchronous motor

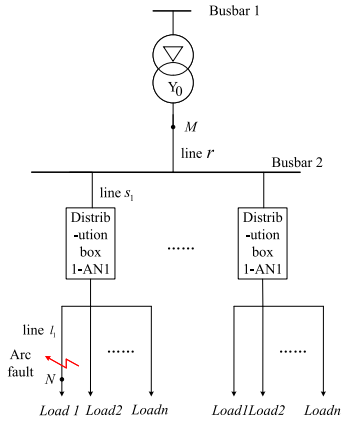

FIGURE 6. Residential building power distribution network.

starting. Therefore, selecting a larger reliability coefficient can ensure that the detection will not mal-operate during normal operation of the distribution network, and will not affect the accuracy of fault detection. The reliability coefficient in this paper is taken as 2.

Specifically, the Hausdorff distance H value between the asynchronous motor startup waveform and the standard sine waveform can be calculated through extensive experiments. Based on the experimental results, the specific value of the detection threshold H_{set} will be determined. This process aims to effectively achieve the logical judgment mentioned above.

3) $\triangle T$ SETTING

Short-time overcurrent release are the devices used in distribution networks to protect lines and equipment from the harmful effects of short-circuit currents. They automatically disconnect the circuit after a certain time delay. The purpose of this time delay is to achieve coordinated operation between upstream and downstream circuit breakers, preventing from override tripping. The operation time t of a short-time overcurrent relay typically has three settings: 0.2 seconds, 0.4 seconds, and 0.6 seconds. These settings can be chosen and adjusted based on different protection requirements.

The design of the action delay Δt for arc fault alarms should be coordinated with the operation time t of the short-time overcurrent release to avoid to be triggered by general faults. The action delay Δt is designed as $\Delta t = t + 0.2$ seconds.

V. SIMULATION VERIFICATION

A. SIMULATION MODEL

Take a residential building distribution networks as an example, a simulation model is established based on Matlab/Simulink for the purpose of conducting simulation experiments on the proposed arc fault detection method. The simulation is carried out according to the configuration of the residential building distribution feeder diagram shown in Figure 6. The 1st outgoing line of the 1st distribution panel is selected as the test object. Table 2 and Table 3 provide the parameters of the line impedance and the types of test loads.

TABLE 2. Main parameters of test cable.

Line	Length(m)	Bore size(mm^2)	Resis-tance(/km)	inductance (mH/km)
l_1	100	4	0.5	100
s_1	100	10	0.16	95
r	100	16	0.1	80

TABLE 3. Main parameters of test load.

Load	Type	Power (W)	Power factor	identi-fication
Electric heater	Resistive	1000	1	A
Induction cooker	inductive	1800	0.87	B
Water heater	Resistive	3000	1	C
Vacuum cleaner	Nonlinear (Series motor)	1300	0.87	D
Air conditioner	Nonlinear (Asynchronous motor)	4000	0.80	E

Conducting arc fault simulations in MATLAB/Simulink based on the Cassie arc model. The model is based on a 220V, 50Hz power supply and includes harmonic sources of 3rd, 5th, and 7th order with RMS values of 5V, 3V, and 2V, respectively. Each harmonic source has an initial phase angle of $\pi/6$, $\pi/3$, and $\pi/2$, respectively. The voltage transducer operates at a sampling frequency of 10kHz. The simulation of series arc faults is carried out using the Cassie arc model.

B. VERIFICATION OF VOLTAGE SAG CHARACTERISTICS

First, the voltage sag scenario in the load access is tested. Before the load access, the branch l_1 is unloaded, and then the test load specified in Table 3 is connected to the branch l_1. Record the voltage values at the load side before and after load access. The voltage sag values before and after access are shown in Figure 9.

Apply a series arc fault in branch l_1 and record the load side voltage waveform and voltage sag values before and after the arc fault occurs under different load conditions. Simulate an arc fault occurring at 0.06 seconds and obtain the load side voltage waveform as shown in Figure 7. The voltage sag value during the fault and the voltage sag value during load connection are depicted in Figure 8.

From Figure 8, it can be observed that before the fault occurs, the load side voltage waveform is a standard sine wave. After the fault, the load side voltage waveform deviates from the sine wave, exhibiting a step-like or distorted pattern at a certain point in the voltage waveform. The waveform characteristics are diverse from each other among various load types. Based on Figure 8, it is evident that in the scenario of load access, except for the asynchronous motor starting, the voltage sag values are relatively small. Among them, the smallest sag value is U_{sag} = 4.22V for load A access, and

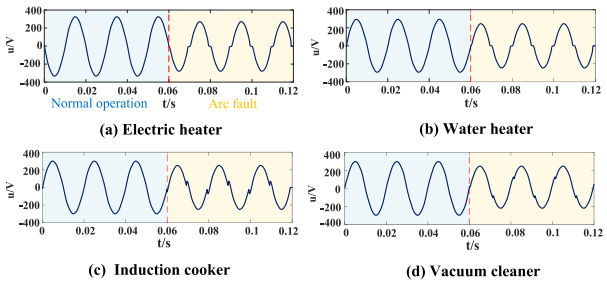

FIGURE 7. Load side voltage waveform of series arc fault.

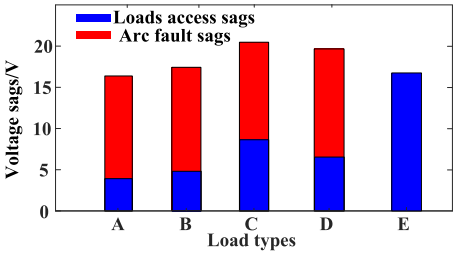

FIGURE 8. Comparison of the voltage sags of series arc fault and load access.

the largest sag value is U_{sag} = 8.13V for load C access, both of which are smaller than the threshold. However, during asynchronous motor starting, the load side voltage sag is U_{sag} = 15.8V, exceeding the threshold.

When an arc fault occurs, despite different load types, the voltage sag values before and after the fault are similar, ranging from 15 to 20V. Among them, the smallest voltage sag during an arc fault is U_{sag} = 16.24V for load A, and the largest is U_{sag} = 20.84V for load C. The voltage sag during an arc fault is higher than the sag values during the access of loads A to D, and it is similar to the voltage sag during the starting of load E. The voltage sag during the starting of load E and during an arc fault is both greater than the given threshold U_{set}.

Based on the above analysis, it can be concluded that the voltage sag values during the load access are all smaller than the start threshold, indicating that the detection procedure will not be triggered. On the other hand, both the asynchronous motor starting and the occurrence of an arc fault result in voltage sag values greater than the start threshold, triggering the detection. Using the load side voltage sag as the detection start condition ensures that detection is not triggered during normal operations, except for asynchronous motor starting.

C. VERIFICATION OF ARC FAULT DETECTION METHOD BASED ON HAUSDORFF DISTANCE ALGORITHM

1) PARAMETER SETTINGS

The fault characteristics of the load side voltage during an arc fault mainly manifest as local distortion features. To capture the localized fault features, it is of importance not to choose an excessively large data window for calculating the Hausdorff distance. Otherwise, the localized features of the fault waveform might not be adequately reflected.

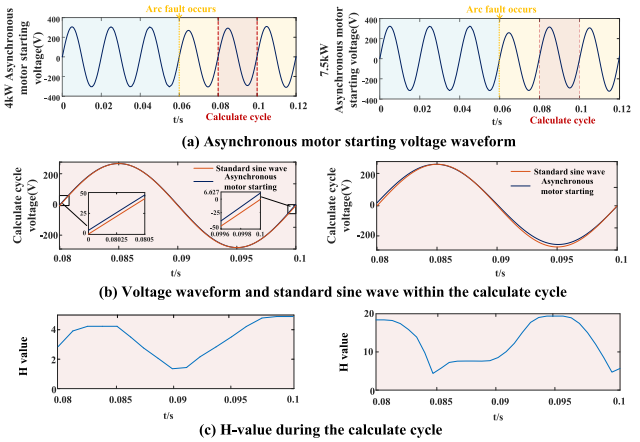

FIGURE 9. H value of starting voltage of three-phase asynchronous motor.

The data window for calculating the Hausdorff distance is chosen as 0.05 cycles, which corresponds to 1 ms. Through experimental comparisons, this data window length effectively captures the localized waveform features while maintaining stable outputs for the detection algorithm.

2) STARTING OF THREE-PHASE ASYNCHRONOUS MOTOR

Using the Hausdorff distance algorithm to detect arc faults involves several steps. First, calculate the Hausdorff distance of the voltage waveform during the starting of a three-phase asynchronous motor. Next, calculate the Hausdorff distance when an arc fault occurs. Finally, compare the calculated Hausdorff distances of these two scenarios and set the detection threshold accordingly.

The three-phase asynchronous motor is started using the direct starting method with the maximum starting current, leading to a significant voltage sag during the starting process. This can lead to false detection. In general, motors with small power (less than 7.5 kW) and infrequent starts are allowed to be directly started. Therefore, in the simulation, two different power motors, one with 4 kW and 1430 RPM, and the other with 7.5 kW and 1440 RPM, will be subjected to direct starting tests.

Figure 9(a) depicts the A-phase voltage waveform during the asynchronous motor starting process. Upon observing the waveform, it can be noticed that the phase voltage gradually recovers during the motor's starting process, exhibiting some fluctuations in amplitude during the recovery. This phenomenon is attributed to the fact that the rotor electromotive force is initially small during the start, resulting in significant amplitude of phase current. Consequently, the line voltage drop is substantial, leading to a smaller amplitude of the load side voltage. As the motor's speed increases, the rotor electromotive force also rises, eventually approaching the load side voltage. As a result, the fluctuations in the amplitude of the motor's phase voltage decrease gradually, ultimately keeping unchanged. For calculating the Hausdorff distance, the voltage waveform of the subsequent period after the occurrence of the voltage sag is selected. During this period,

the amplitude fluctuations are small, and the waveform is relatively stable.

Figure 9(b) illustrates the voltage waveform of the subsequent period after the voltage sag occurrence, along with the reference sinusoidal waveform that matches the amplitude of the voltage waveform. It is evident from the figure that the two waveforms exhibit high similarity in their shapes.

Figure 9(c) depicts the calculated results of the Hausdorff distance for the selected computation period. The Hausdorff distance calculated between the voltage waveform and the reference sinusoidal waveform is referred to as the H-value. The results indicate that the H-value output remains stable after the asynchronous motor starts. For the 4kW asynchronous motor, the maximum computed period H-value is 4.81, while for the 7.5kW asynchronous motor, the maximum computed period H-value is 19.63. It is evident that the larger the motor's power, the greater the computed H-value within the calculation period. Since the maximum starting power for the direct starting method is typically limited to 7.5kW, the most unfavorable factor for detection shall be the 7.5kW asynchronous motor's start-up, its maximum H-value during starting process is 19.63.

Based on the above results, the detection threshold for the Hausdorff distance is set to H_{set} = 39.26. It should be noted that this is the detection threshold of the preliminarily setting, and the detection effect of this threshold needs further simulation and test. If the detection effect is not good, it is necessary to further modify this threshold to meet the requirements of fault detection.

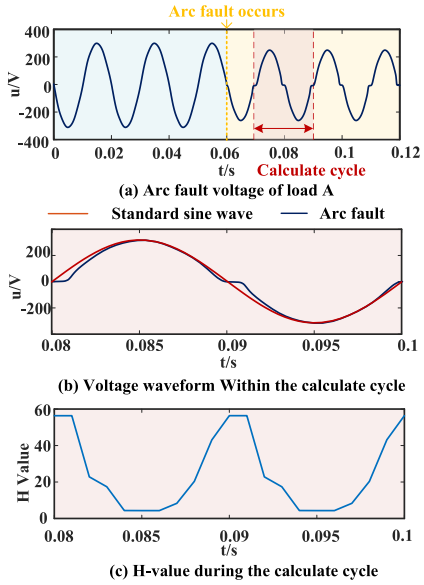

FIGURE 10. H value of voltage of series arc fault.

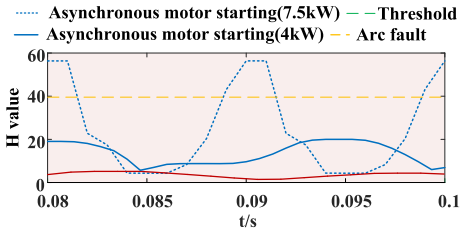

FIGURE 11. Comparison of the H value of three-phase asynchronous motor starting and series arc fault.

3) SERIES ARC FAULT

Based on the conclusions drawn from the analysis of arc fault waveform characteristics in Section V-B, it is evident that the fault characteristics are more prominent in nonlinear and inductive loads, while resistive loads exhibit less distinct fault characteristics. To ensure the sensitivity of detection, the case that an arc fault occurs in resistive load A with the least distinct fault characteristics, is selected as the most unfavorable scenario for the purpose of detection. In this scenario, the H-value of the load side voltage after the occurrence of an arc fault in resistive load A is calculated.

Figure 10(a) illustrates the voltage waveform during an arc fault occurrence in a resistive load A. In the initial stage of the fault, the voltage amplitude drops to a lower level when the arc is conducting, and there is a certain "zero rest" time during voltage zero crossings. The voltage waveform in the subsequent period after the occurrence of the arc fault is chosen to calculate its Hausdorff distance.

Figure 10(b) illustrates the voltage waveform of the subsequent period after the voltage sag along with the template sinusoidal waveform. There is a noticeable "zero rest" time in the fault voltage at the load side, and there is a distinct waveform disparity compared to the standard sinusoidal waveform.

Figure 10(c) illustrates the computed results of the Hausdorff distance for the selected calculation period. The results reveal that during the fault at the load terminal voltage within the calculation period, the voltage at the load side remains at 0V for approximately 0.1 cycles around the zero-crossing time. Within this window, the voltage waveform significantly deviates from the template sinusoidal waveform, resulting in the maximum H value of 56.35. When the voltage at the load side reaches its peak value, the voltage matches the amplitude of the template sinusoidal waveform, yielding the minimum H value of 4.32. The maximum and minimum H values repeat twice within a single cycle.

4) VERIFICATION OF DETECTION EFFECT

Figure 11 compares the magnitudes of H values during the asynchronous motor starting process and during the occurrence of a series arc fault. As shown, it is evident that the H value during a series arc fault is significantly greater than that during asynchronous motor starting. The H value during a series arc fault oscillates periodically between 4.32 and 56.35. Within a single cycle of H value calculate result $H = [H_1, H_2, \cdots, H_{20}]$, there are five data points that exceed the detection threshold H_{set}. Additionally, every half cycle, there is one occurrence of H value exceeding

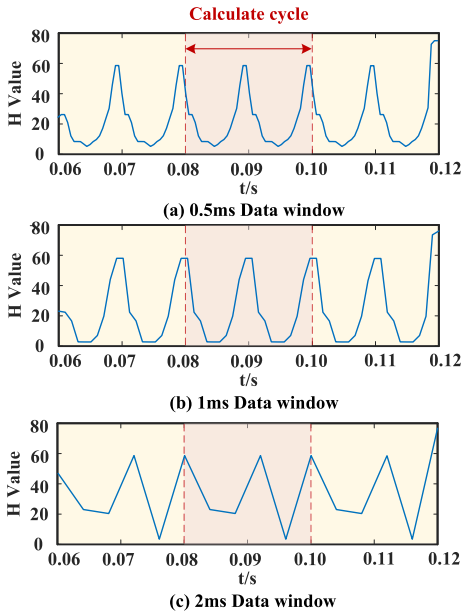

FIGURE 12. Arc detection with different data windows.

the threshold. According to the detection procedure, this indicates the presence of an arc fault. On the other hand, the H value during asynchronous motor starting remains consistently below the detection threshold H_{set}, avoiding the frequent pick-up due to motor starting.The above simulation results show that the threshold setting of the preliminary setting threshold is reasonable and is able to identify arc fault.

Set resistive arc faults in the line, and simulate the change of H value under different data window lengths as shown in Figure 12. As can be seen from Figure 12, the fluctuation of H value is greater when the data window is long. Among them, the large data window length of Figure12(c) can no longer reflect the periodic fault characteristic of arc voltage. This is because the data window contains both zero rest area and sine wave area. It can also be seen that the smaller the data window, the better the algorithm reflects the partial features. However, the smaller the data window, the higher the requirement for sampling frequency. Excessive sampling rate will increase the application cost of the method, which is not conducive to engineering practicality. Therefore, under the condition that both 0.5ms and 1ms data windows can output stable H values and reflect the periodic fault characteristic of arc voltage, the 1ms data window was ultimately selected to reduce the sampling rate requirement of the method.

5) COMPARISON WITH SIMILAR METHODS

In order to demonstrate the superiority of the proposed method, a comparative experiment was conducted between the method presented in this paper and the traditional current-based arc fault detection method.

To capture the local characteristics of arc fault waveforms, existing arc fault detection techniques typically employ time domain or time-frequency domain methods to detect series arc faults. In reference [13], two cycles of current from the electrical circuit are collected, and the "zero rest" time ratio coefficient is calculated, which serves as a fault feature. Reference [12] proposes a diagnostic method that utilizes DWT(Discrete Wavelet Transform) to extract the frequency range of fault features, with the extracted feature being the d3 component from 2 to 4 kHz obtained from db2 wavelet decomposition. Reference [15] employs EMD (Empirical Mode Decomposition) to extract IMF (Intrinsic Mode Function) components that reflect the local characteristics of arc fault signals. These IMF components are then used as fault features for fault diagnosis.

In the comparative experiment, this paper will assess the performance of the aforementioned detection methods. The selected fault features and their criteria are outlined in Table 4.

TABLE 4. Types of fault criterion.

Fault feature	Feature type	Reference
Scale of zero rest time	Time domain	[13]
DWT Frequency band of d3(2-4kHz)	Time-frequency domain	[12]
EMD's IMF1-IMF7 component	Time-frequency domain	[15]
Voltage sags & Hausdorff distance	Time domain	/

The simulation of arc fault was carried out in the experimental conditions built in Section V-A, included a total of 50 cases, covering various fault scenarios and load types, to thoroughly assess the performance of the four methods. In these simulations, all four methods demonstrated effective arc fault identification and no instances of missed detection were observed.

However, the comparative criteria exhibited poor reliability in normal operating conditions, resulting in four cases where normal operation was incorrectly classified as an arc fault. The scenarios with incorrect results are presented in Table 5, the working current waveforms of these loads are shown in Figure 16. In the table, "√" represents accurate detection of normal operation, while "×" indicates misjudgment for normal operation.

TABLE 5. Misclassification scenario of normal operation.

Loads type	[13]	[12]	[15]	This paper
Electronic dimmer & tungsten lamp 300W	×	×	√	√
Microwave oven 1000W	√	√	×	√
Electric hand drill 1000W	×	√	√	√
Switch power supply 300W	×	×	√	√

The electronic dimmer and the switch power supply belong to the power electronic load. The working current of the above-mentioned power electronic loads have a relatively obvious zero rest time. This waveform feature has caused the literature [12] and literature [13], which identify arc faults by detecting partial waveform distortions, to misjudge. Compared with the power electronic load,

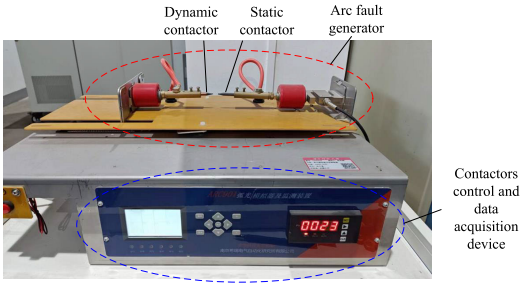

FIGURE 13. Series arc generator and data monitoring device.

the zero rest time of the hand drill is shorter, causing the method in literature [12] to misjudge, and literature [13] did not misjudge. The working current of the microwave oven contains complex harmonic content and nonlinear components, causing the literature [15] that identifies arc faults by detecting nonlinear and non-stationary signals to misjudge.

However, the method proposed in this paper did not misjudge when the load was operating normally. This is because the voltage sag values when the above loads access is 0.92V, 2.98V, 3.02V, and 0.90V, respectively, which are lower than the detection start threshold of 10.8V, and the detection does not start reliably. Therefore, the method proposed in this paper shows extremely high reliability when the load is operating normally.

From the simulation results, it can be concluded that: 1) Traditional current-based arc fault detection methods are capable of accurately detecting arc faults. However, due to the diverse current profiles of non-linear loads, these methods struggle to differentiate between fault currents and currents associated with non-linear loads such as motors and power electronics-type loads. This limitation can lead to misjudgment. 2) The detection method proposed in this paper outperforms traditional arc fault detection methods in terms of reliability. It effectively distinguishes between arc faults and the operation of nonlinear loads. By using the proposed detection method, the accuracy of detection has been improved.

D. TEST VERIFICATION

With the support of the "Intelligent Distribution Network Physical Dynamic Simulation Platform" established by the author's affiliated institution, this paper conducted experimental testing on series arc faults under different loads. The series arc fault testing platform consists of a power supply, a series fault arc generator, precise control devices for switch operation and closing, a load, data acquisition and monitoring equipment, and a PC, as shown in Figures 13 and 14. The series arc fault generator is constructed in accordance with the standard GB/T 31143-2014 and GB 14287.4-2014. It can achieve precise adjustment of the gap between dynamic and static contactors through a precision stepper motor control, enabling the simulation of different series arc discharge processes and flexible setting of parameters such as discharge

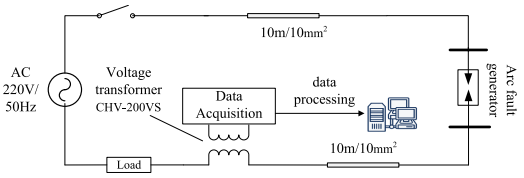

FIGURE 14. Series arc fault test system.

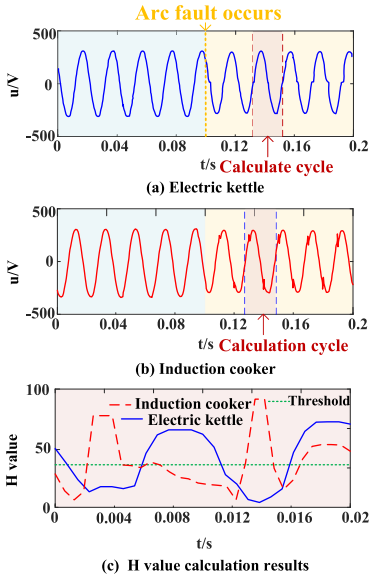

FIGURE 15. Calculation results of Hausdorff distance between electric kettle and induction cooker.

duration, discharge frequency, and discharge intervals. The voltage sensor uses a closed-loop Hall sensor with a model number of CHV-200VS, measuring a range of 0 to ±300V, with a frequency measurement bandwidth of 20kHz, which can be used for electrical quantity monitoring and data acquisition in the arc discharge circuit.

The loads for the arc fault tests are shown in Table 6. The tests were conducted with an arc fault occurrence time of 0.1 seconds. Figure 14 illustrates the voltage waveform at the load side and the calculated H-value after arc faults occurred in an electric kettle and an induction cooker. Due to space limitations, the test results for other loads are presented in Table 7.

TABLE 6. Main parameters of test load.

Load	Type	Power (W)	Power factor
Electric kettle	Resistive	800	1
Induction cooker	Inductive	1800	0.87
Electric bicycle charger	Nonlinear(Switch power supply)	300	0.92
Hair drier	Nonlinear(Series motor)	1000	0.80

From the fault waveforms in Figure 15(a) and Figure 15(b), it can be observed that due to the randomness and instability of arc faults, there is a certain degree of voltage waveform

TABLE 7. Fault detection test results.

Load	Fault sag(V)	$H_{\max}$	Threshold exceeding times	Detection result
Electric kettle	19.3	65.53	3	Fault
Induction cooker	20.2	91.56	3	Fault
Electric bicycle charger	18.6	71.89	4	Fault
Hair drier	19.1	82.45	3	Fault

jitter. The fault characteristics of the load-side voltage during the experiments are more complex compared to the simulation results. The H value calculation results in Figure 14(c) indicate that the H values for the electric kettle load exceed the threshold three times within one cycle, and the induction cooker also exceeds the threshold three times, both of which are detected as arc faults.

Analyzing the fault waveforms and H value calculation results, it can be concluded that the actual arc sustaining process is unstable, with voltage waveforms at the load side experiencing random fluctuations and singularities during the arc's persistence. This leads to larger H values and a higher number of H value threshold exceedances within the calculation cycle compared to the simulation results. This instability is advantageous for the detection and recognition of faults.

To further validate the effectiveness of the detection method, fault recognition experiments were conducted for all loads listed in Table 6, and the experimental results are presented in Table 7.

The voltage sag of the arc fault in the test is around 20V, which is consistent with the results of theoretical and simulation analysis. In the test, the voltage sag of the arc fault in the electric bicycle charger is the smallest, and the voltage drop value of the arc fault in the induction cooker is the largest, which is 20.2V and 20.8V. In comparison, the minimum value of the fault drop in the simulation is 15.8V, and the maximum value is 18.6V. Comparing the above results, we can draw the following conclusions: First, the simulation results of the arc fault drop indicate that the arc fault drop should be between 15-20V. The test results verify this conclusion, and the startup threshold U_{set}=10.8V can ensure reliable start when an arc fault occurs. Second, the distribution of fault sag values under different loads in the test is more concentrated, which will be beneficial to the reliable start of this method in practical applications.

To sum up, the test results demonstrate that the voltage sags for all tested loads meet the startup conditions, and the number of H value threshold exceedances within the calculation cycle satisfies the fault discrimination criteria. Therefore, the proposed detection method can accurately identify arc faults under different load types, making it applicable for series arc fault detection in real distribution lines. Meanwhile, the test results show that the preliminary setting threshold can effectively detect fault arcs without further modification and the detection threshold H_{set} finally set as 39.26.

VI. CONCLUSION

Aiming at the limitations of existing series arc fault current detection methods, particularly their vulnerability in the case of the operation of nonlinear loads, a novel series arc fault detection method is proposed, which relies on voltage sag characteristics and the Hausdorff distance algorithm. The following conclusions have been drawn as below:

1) The voltage sag amplitudes during arc faults are similar for various load types. The proposed arc fault detection method based on voltage sag characteristics outperforms traditional methods that rely on wave-form features. This is because that the proposed method avoids judgment leakage and misjudgment caused by the diverse waveform characteristics of arc faults. However, it should be noted that the voltage sag criterion might lead to misjudgment during asynchronous motor starting due to the significant voltage sag occurring during this stage.

2) To differentiate between asynchronous motor starting and arc faults, the Hausdorff distance algorithm is employed to quantify the distortion of load side voltage. Simulation results demonstrate that the Hausdorff distance of load side voltage during arc faults is significantly higher than that during asynchronous motor starting. Thus, the introduction of the Hausdorff distance algorithm effectively addresses the identification challenge between asynchronous motor starting and arc faults. This enhancement improves the detection method and enhances its reliability.

3) The detection performance of the proposed method is compared with mainstream fault detection techniques. Experimental results show that traditional arc fault detection methods struggle to balance sensitivity and reliability. The dual criteria of voltage sag and Hausdorff distance introduced in this paper accurately capture fault characteristics, leading to an improved detection accuracy.

4) Experimental validation of the proposed detection method was conducted using the "Intelligent Distribution Network Physical Dynamic Simulation Platform." The test results indicate that the proposed method can accurately identify arc faults under different load types and is suitable for practical series arc fault detection in distribution circuits.

APPENDIX
THE CURRENT WAVEFORMS THAT CAUSED MISJUDGMENTS IN TABLE 5

See Figure 16.

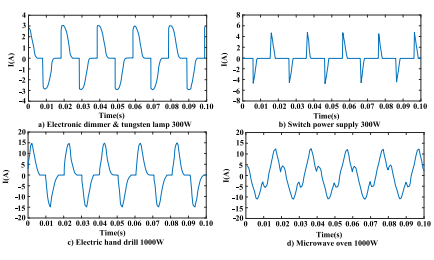

FIGURE 16. Current waveforms that caused misjudgments.

REFERENCES

[1] H. Wang, Y. Shen, Y. Niu, and Y. Zheng, "Design and research of building automation system and its system planning for green intelligent building," *J. Environ. Prot. Ecol.*, vol. 20, no. 2, pp. 932–941, Jan. 2019.
[2] *UL Standard for Safety for Arc Fault Circuit Interrupter*, Standard UL1699, 2008.
[3] *Electrical Fire Monitoring systemPart 4: Arcing Fault Detectors*, Standard GB 14287.4-2014, 2014.
[4] A. Ghaderi, H. A. Mohammadpour, H. L. Ginn, and Y.-J. Shin, "High-impedance fault detection in the distribution network using the time-frequency-based algorithm," *IEEE Trans. Power Del.*, vol. 30, no. 3, pp. 1260–1268, Jun. 2015.
[5] J. Yuventi, "DC electric arc-flash hazard-risk evaluations for photovoltaic systems," *IEEE Trans. Power Del.*, vol. 29, no. 1, pp. 161–167, Feb. 2014.
[6] C. E. Restrepo, "Arc fault detection and discrimination methods," in *Proc. 53rd IEEE Holm Conf. Electr. Contacts*, Pittsburgh, PA, USA, Sep. 2007, pp. 115–122.
[7] G. Parise and P. A. Scarpino, "A basic assessment of arc flash in low voltage AC," *IEEE Trans. Ind. Appl.*, vol. 57, no. 5, pp. 4513–4519, Sep. 2021.
[8] G. Artale, A. Cataliotti, V. Cosentino, D. Di Cara, S. Nuccio, and G. Tinè, "Arc fault detection method based on CZT low-frequency harmonic current analysis," *IEEE Trans. Instrum. Meas.*, vol. 66, no. 5, pp. 888–896, May 2017.
[9] M. S. Mamiş and M. E. Meral, "State-space modeling and analysis of fault arcs," *Electric Power Syst. Res.*, vol. 76, nos. 1–3, pp. 46–51, Sep. 2005.
[10] G. Parise, L. Martirano, and R. E. Nabours, "Arc-fault protection of branch circuits, cords, and connected equipment," *IEEE Trans. Ind. Appl.*, vol. 40, no. 3, pp. 896–899, May 2004.
[11] P. Qi, S. Jovanovic, J. Lezama, and P. Schweitzer, "Discrete wavelet transform optimal parameters estimation for arc fault detection in low-voltage residential power networks," *Electr. Power Syst. Res.*, vol. 143, pp. 130–139, Feb. 2017.
[12] K. Koziy, B. Gou, and J. Aslakson, "A low-cost power-quality meter with series arc-fault detection capability for smart grid," *IEEE Trans. Power Del.*, vol. 28, no. 3, pp. 1584–1591, Jul. 2013.
[13] H. Zhao, J. Liu, and J. Lou, "Series arc fault detection based on current fluctuation and zero-current features," *Electr. Power Syst. Res.*, vol. 202, Jan. 2022, Art. no. 107626.
[14] W. Luan, J. Lin, B. Liu, and B. Zhao, "Arc fault detection and identification via non-intrusive current disaggregation," *Electr. Power Syst. Res.*, vol. 210, Sep. 2022, Art. no. 108113.
[15] F. Guo, H. Gao, Z. Wang, J. You, A. Tang, and Y. Zhang, "Detection and line selection of series arc fault in multi-load circuit," *IEEE Trans. Plasma Sci.*, vol. 47, no. 11, pp. 5089–5098, Nov. 2019.
[16] H. Gao, Z. Wang, A. Tang, C. Han, F. Guo, and B. Li, "Research on series arc fault detection and phase selection feature extraction method," *IEEE Trans. Instrum. Meas.*, vol. 70, pp. 1–8, 2021.
[17] A. Chabert, M. C. Bakkay, P. Schweitzer, S. Weber, and J. Andrea, "A transformer neural network for AC series arc-fault detection," *Eng. Appl. Artif. Intell.*, vol. 125, Oct. 2023, Art. no. 106651.
[18] R. Jiang, Y. Wang, X. Gao, G. Bao, Q. Hong, and C. D. Booth, "AC series arc fault detection based on RLC arc model and convolutional neural network," *IEEE Sensors J.*, vol. 23, no. 13, pp. 14618–14627, Jul. 2023.
[19] H. Bai and Z. Xu, "Arc fault identification method based on wavelet packet transform and high-order cumulant," *Electr. Power Autom. Equip.*, vol. 40, no. 11, pp. 195–202, Nov. 2023.
[20] J. C. Kim, D. O. Neacsu, B. Lehman, and R. Ball, "Series AC arc fault detection using only voltage waveforms," in *Proc. IEEE Appl. Power Electron. Conf. Expo. (APEC)*, Anaheim, CA, USA, Mar. 2019, pp. 2385–2389.
[21] W. Wang, B. Xu, and Z. Sun, "Differential voltage method for arc fault detection in low voltage distribution networks," *Proc. CSEE*, vol. 1, pp. 1–14, May 2023.
[22] C. Han, Z. Wang, A. Tang, H. Gao, and F. Guo, "Recognition method of AC series arc fault characteristics under complicated harmonic conditions," *IEEE Trans. Instrum. Meas.*, vol. 70, pp. 1–9, 2021.
[23] R. Holm, *Electric Contacts Theory and Application*. Berlin, Germany: Springer, 2013, pp. 40–48.
[24] G. Bizjak, P. Zunko, and D. Povh, "Circuit breaker model for digital simulation based on Mayr's and Cassie's differential arc equations," *IEEE Trans. Power Del.*, vol. 10, no. 3, pp. 1310–1315, Jul. 1995.
[25] M. H. Bollen, *Understanding Power Quality Problemsvoltage Sags and Interruptions*. Piscataway, NJ, USA: IEEE Press, 1999.
[26] D. L. Brooks, R. C. Dugan, M. Waclawiak, and A. Sundaram, "Indices for assessing utility distribution system RMS variation performance," *IEEE Trans. Power Del.*, vol. 13, no. 1, pp. 254–259, Jan. 1998.
[27] N. Matanov, "Study of the impact of induction motors starting on the supply voltage," in *Proc. 16th Conf. Electr. Mach., Drives Power Syst. (ELMA)*, Varna, Bulgaria, Jun. 2019, pp. 1–5.
[28] A. Wang, X. Sun, X. Zhou, and W. Hu, "A study of voltage sags in electric motors," in *Proc. Chin. Control Decis. Conf. (CCDC)*, Mianyang, China, Aug. 2011, pp. 4270–4272.
[29] J. J. Perez, C. A. Cortes, and A. Gomez, "Difference squared Hausdorff distance based medical image registration," in *Proc. 9th Int. Conf. Elect. Power Quality Utilisation*, Varna, Bulgaria, Oct. 2007, pp. 1–6.

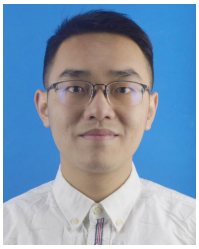

KAIJIE WANG received the B.S. degree in electrical engineering from North China Electric Power University, Baoding, China, in 2022. He is currently pursuing the master's degree in electrical engineering with the Huazhong University of Science and Technology (HUST), Wuhan, China. His main research interests include arc fault detection and power system protective relay.

XIANGNING LIN (Senior Member, IEEE) was born in Guangxi, China, in 1970. He received the M.S. and Ph.D. degrees in electrical engineering from the Huazhong University of Science and Technology (HUST). Currently, he is a Full Professor with HUST. His research interests include microgrid scheduling, modern signal processing, and power system protective relay.

FANRONG WEI received the Ph.D. degree in electrical engineering from the Huazhong University of Science and Technology (HUST). His research interests include optimal power system/microgrid scheduling and protective relay.

HU WEI was born in 1981. She received the Ph.D. degree in electrical engineering from the Huazhong University of Science and Technology (HUST). Currently, she is a Senior Engineer with the State Grid Hubei Electric Power Research Institute. Her research interests include analysis of distribution network operation, application of AC/DC hybrid distribution networks, and power electronics technology in distribution networks.